MJFAS
Malaysian Journal of Fundamental and Applied Sciences

Osman *et al.* | Malaysian Journal of Fundamental and Applied Sciences, Vol. 21 (2025) 2870–2888

RESEARCH ARTICLE

Tailoring the pH-responsive Properties of Titania Nanocomposite Functionalized with Polymethacrylic Acid for the Photodegradation of Paracetamol

Elis Osman[a], Sheela Chandren[a,b*], Yoki Yulizar[c], Nor Arbani Sean[a]

[a]Department of Chemistry, Faculty of Science, Universiti Teknologi Malaysia, 81310 UTM Johor Bahru, Johor, Malaysia; [b]Centre for Sustainable Nanomaterials, Ibnu Sina Institute for Scientific and Industrial Research, Universiti Teknologi Malaysia, 81310 UTM Johor Bahru, Johor, Malaysia; [c]Department of Chemistry, Faculty of Mathematics and Natural Sciences, Universitas Indonesia, Depok 16424, Indonesia

Abstract In this work, the free radical polymerization (FRP) method was employed to create pH-responsive polymethacrylic acid-titania nanocomposites (PMAA-TiO_2 NCs) for the efficient photocatalytic degradation of paracetamol, a commonly used analgesic and antipyretic known as acetaminophen. The environmental risk posed by the accumulation of paracetamol in the food chain underscores the need for effective water treatment solutions. The need to address potential environmental toxicity prompted a meticulous investigation of TiO_2 and crosslinker (CL) concentrations on PMAA, with X-ray diffraction (XRD) confirming anatase and rutile phases. Fourier transform infrared (FTIR) spectra validated distinctive functional groups, and ultraviolet-visible near-infrared (UV-vis-NIR) spectroscopy determined bandgap energy alignment within the anatase TiO_2 range. Field emission scanning electron microscopy (FESEM) revealed seamless integration of PMAA with TiO_2 nanoparticles, displaying a size distribution of 35 to 80 nm. Thermogravimetric analysis (TGA) demonstrated polymer degradation at 300 – 500 °C. Notably, the pH-dependent photocatalytic efficiency showed optimal TiO_2 (0.4 g) and CL (0.7 g), achieving 60.3% removal efficiency in basic conditions and 21.1% in acidic conditions under UV light. This pH-responsive behavior was attributed to the swelling effect of PMAA under basic conditions, which increased the surface area and provided more active sites for photocatalysis. The PMAA layer's ionization in basic environments led to a highly negatively charged surface, facilitating greater interaction with reactive oxygen species (ROS) and enhancing photocatalytic performance. These results highlight PMAA's crucial role in imparting pH responsiveness to TiO_2, emphasizing its significance in environmental remediation.

Keywords: Photocatalyst, Titania, Polymethacrylic Acid, Free Radical Polymerization, Paracetamol.

***For correspondence:**
sheela@utm.my

Received: 3 July 2025
Accepted: 3 Sept. 2025

Introduction

TiO_2 nanoparticles (TiO_2 NPs) stand as a cornerstone in the realm of photocatalysis, presenting themselves as a naturally occurring oxide with remarkable properties [1]. TiO_2, particularly in the anatase form, exhibits unparalleled photocatalytic activity, making it a promising agent for the elimination of environmental pollutants [2]. The advantages of TiO_2, including non-toxic characteristics, chemical stability [3], environmental friendliness, and low cost, have propelled its extensive application in various fields, from construction materials [4] to wastewater treatment [5]. Despite these commendable attributes, the practical use of TiO_2 faces challenges, particularly in harnessing solar energy for photocatalysis and optimizing its catalytic efficiency due to rapid charge carrier recombination. Generally, TiO_2 demonstrates limited photocatalytic activity in visible light due to its relatively wide bandgap (E_g) (~3.2 eV), which falls within the Ultraviolet (UV) radiation range (100 – 400 nm) [6]. Due to this restriction, TiO_2 can only use around 5% of the solar energy [7]. On the other hand, the acidity and basicity of surface

sites can also significantly influence the catalytic performance of TiO_2 [8]. In regard to these two points, the photocatalytic activity of TiO_2 NPs cannot be fully maximized since it has a low adsorption capacity and is not sensitive to pH changes.

Various systems have been developed for the specific photodegradation of paracetamol using heterogeneous photocatalysts. Advanced oxidation processes involving TiO_2 combined with hydrogen peroxide (H_2O_2) have been utilized to generate reactive oxygen species, enhancing paracetamol degradation [9]. Although effective, these methods are often costly and require tight control of reaction conditions. Other studies have explored alternative photocatalysts, such as zinc oxide (ZnO) and iron oxides (Fe_2O_3), which have shown improved degradation rates. Nevertheless, challenges such as instability and poor responsiveness to pH variations persist [10, 11]. Pure TiO_2 has also been employed for paracetamol degradation, achieving moderate efficiencies of 40 – 60 % under UV light [12]. However, TiO_2 systems generally suffer from pH insensitivity, which limits their performance across different environmental conditions.

In the dynamic domain of photocatalytic processes, the imperative fusion of pH-responsive attributes into photocatalysts stands as an essential pursuit. This synergistic amalgamation assumes profound importance, acting as a catalyst to elevate the selectivity and precision of the photocatalyst amidst a myriad of reactions [13]. The integration of pH-responsive functionalities emerges as a pivotal cornerstone, enabling a meticulously orchestrated release of active species in harmony with the subtleties of kinetics and reaction mechanisms [14]. This refined control enhances the catalytic process and maximizes the photocatalyst's overarching efficiency [15]. Therefore, this study aims to address these limitations through a synthesis approach that involves incorporating TiO_2 into polymer nanocomposites (PNCs).

PNCs have gained prominence due to their unique physical and chemical properties, enhancing mechanical strength, electrical and thermal conductivity, toughness, and stiffness [16]. Stimuli-responsive polymers are one type of smart material due to the unique ways they react to external stimuli such as light, temperature, and pH in various applications [17]. As a result, these polymers change their topography, physical and chemical characteristics. Poly(methacrylic acid) (PMAA) is one of the pH-sensitive polymers with carboxylic acid groups that respond to changes in pH. The pKa value of PMAA is 6.0, indicating that it is a weak polyacid [18]. PMAA can swell in basic environments due to the electrostatic repulsion between deprotonated –COOH [19]. On the other hand, PMAA has the potential to shrink in acidic conditions due to the protonation of the COO^- groups.

The swelling effect of PMAA occurs significantly under specific reaction media, particularly in an alkaline condition [20]. The PMAA may behave like a highly water-swollen material in an alkaline suspension, which induces high surface area and permeability to reaction substrates. As a result, the increased surface area in alkaline conditions enhances the accessibility of reactive sites within the polymer matrix, facilitating better interaction between the photocatalyst and the reaction medium. This is hypothesized to contribute to improved photocatalytic activity. Moreover, it has been observed that the basicity of the TiO_2 surface can be improved through surface modification with a polymer. According to Jin *et al.* [21], the stability and basicity of the TiO_2 surface are increased by higher surface charges, resulting in a higher rate of adsorption. This is due to the increasing surface charges after modification, which enhance the intermolecular forces between the carboxylic acid functional group [22]. Therefore, the modification with PMAA can enhance TiO_2 photocatalytic efficiency due to the higher adsorption rate and active sites available for adsorption [23].

In this context, the incorporation of PMAA into TiO_2 serves as a strategic solution to enhance photocatalytic activity, leveraging the pH-responsive nature of PMAA. PMAA-TiO_2 NCs can be synthesized via free-radical polymerization, which involves the polymerization of monomers with low molecular weight in the presence of a cross-linking agent [24]. This research addresses environmental concerns related to the limited biodegradability of pharmaceutical substances, with a specific emphasis on paracetamol. Paracetamol was extensively employed for alleviating headaches, backaches, and rheumatic pain [25]. Its significance in COVID-19 treatment plans globally has led to a surge in its usage, posing an increased risk of environmental release [26]. However, paracetamol exhibits minimal biodegradability, emphasizing the critical need for alternative approaches like employing heterogeneous photocatalysts with TiO_2 [27].

In this work, pH-responsive PMAA-TiO_2 NCs composed of a stimuli-responsive polymer, PMAA, and TiO_2 were synthesized by free radical polymerization (FRP), where the amount of TiO_2 and crosslinker (CL) was varied. The photocatalytic activity of TiO_2 nanoparticles (NPs) was improved by integrating them into pH-responsive polymer nanocomposites (PNCs). Although TiO_2 nanoparticles have limits in

terms of their activity in visible light and sensitivity to pH, these issues can be overcome by using pH-responsive polymers. Poly(methacrylic acid) (PMAA), a polymer that is sensitive to changes in pH, was selected due to its ability to expand and contract in response to pH variations. The PMAA-TiO_2 NCs obtained for each parameter were evaluated for the photocatalytic activity in the photodegradation of paracetamol under UV light irradiation to optimize the amount of TiO_2 and CL used. Next, the PMAA-TiO_2 NCs with the highest and lowest photocatalytic efficacy for each parameter were characterized using various instruments to determine the physicochemical properties, followed by the pH responsiveness test of the PMAA-TiO_2 NCs with the optimum amount of TiO_2 and CL to evaluate their pH-responsive properties in acidic and basic solutions, offering insights into their adaptability for diverse wastewater treatment conditions. The pH-responsiveness test affects the NCs' ability to adapt to varying pH conditions, with different degradation rates observed in several conditions.

Materials and Methods

The reagents titanium(IV) oxide (TiO_2, ≥99.5%), methacrylate acid (MAA, 98%), 2,2′-azobis (2-methylpropionamidine) dihydrochloride (AMPA, 98%), N,N′-methylene-bis-acrylamide (ABM, 96%), sodium hydroxide (NaOH, ≥97%), hydrochloric acid (HCl, 37%), and paracetamol (98%) were purchased from Sigma-Aldrich. Distilled water was used throughout the experiments. All reagents were used without any further purification.

Synthesis of PMAA-TiO_2 NCs

PMAA-TiO_2 NCs were synthesized through free radical polymerization (FRP) in distilled water, employing AMPA as the initiator at a controlled temperature of 65 °C [33]. In the standard polymerization process, 0.2 g of TiO_2 was dispersed in 12 mL of distilled water with ultrasonication assistance for 10 minutes, as depicted in Scheme 1. Subsequently, 0.04 g of the initiator (AMPA) and 0.2 g of ABM were introduced to the mixture, followed by a 15-minute stirring period before transferring to a sealed round-bottom flask. MAA monomer (2 mL) was subsequently added to the mixture during this stage. The mixture underwent a 30-minute nitrogen flow and was immersed in an oil bath at 65 °C for 6 hours [25]. The resulting PMAA-TiO_2 NCs were washed with distilled water to eliminate unreacted substances [35]. The solid product was then left to dry overnight at room temperature. Following the synthesis, the photocatalytic activity of the PMAA-TiO_2 NCs was evaluated by degrading paracetamol under UV light irradiation. To optimize the amount of TiO_2 as the photocatalyst, the weight of TiO_2 nanoparticles was varied. Subsequently, the entire procedure was reiterated, incorporating the optimal TiO_2 amount from the initial study, with varying amounts of CL, as detailed in Table 1.

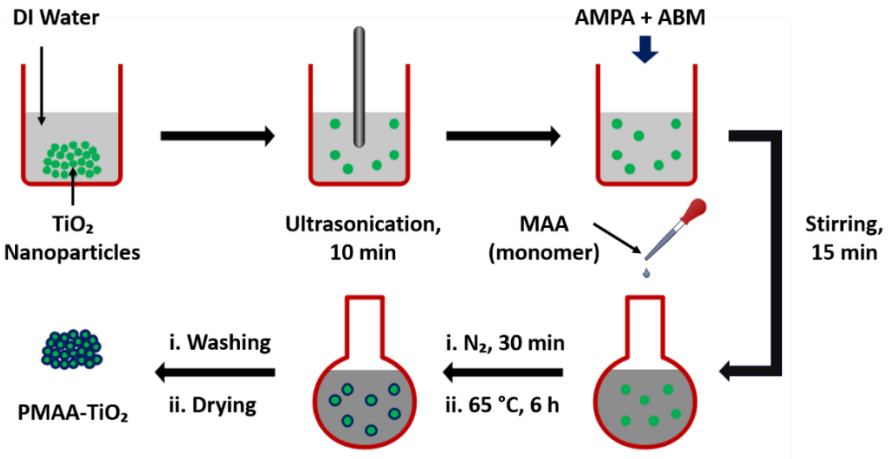

Scheme 1. Schematic illustration of the preparation method of PMAA-TiO_2 NCs.

Table 1. Experimental conditions of the synthesis of PMAA-TiO_2 NCs via FRP in distilled water at 65 °C.

Samples	Amounts		
	TiO_2 (g)	ABM (g)	AMPA (g)
PMAA-TiO_2-0.2	0.2	0.2	0.04
PMAA-TiO_2-0.4	0.4	0.2	0.04
PMAA-TiO_2-0.5CL	0.4	0.5	0.04
PMAA-TiO_2-0.7CL	0.4	0.7	0.04

The TiO_2 loadings (0.2 g and 0.4 g) were selected to compare low and higher photocatalyst contents, where 0.4 g has been reported in prior studies [28] to provide optimal nanoparticle dispersion and light absorption without excessive agglomeration. Similarly, CL concentrations of 0.5 g and 0.7 g were chosen to evaluate the influence of crosslinking density on the rigidity of the PMAA network and the accessibility of TiO_2 active sites, as values in this range have been widely applied in polymer–TiO_2 NCs.

Characterization

PMAA-TiO_2 NCs were characterized using advanced analytical techniques. Fourier-transform infrared spectroscopy (FTIR) was performed with a Perkin-Elmer 1600 instrument in transmittance mode over a wavenumber range of 4000 – 400 cm^{-1}. UV-vis-NIR spectroscopy, conducted using a JASCO V-670 double-beam spectrophotometer, examined electronic transitions within a wavelength range of 200 – 800 nm, with a resolution of 1 – 2 nm. Additionally, UV-vis spectroscopy using a Shimadzu UV-1800 was employed to monitor the photodegradation of paracetamol, analyzing an initial concentration of 25 ppm within the same wavelength range, with a resolution of 1 nm. The surface morphology and particle size of the nanocomposites were investigated via field emission scanning electron microscopy (FESEM) using a JEOL JSM-6701F at an acceleration voltage of 5.0 kV. X-ray diffraction (XRD) analysis was performed with a Bruker D8-Advance diffractometer using Cu K_β radiation (λ = 1.3922 Å) at 40 kV and 30 mA to determine the phase composition and crystallite size of the TiO_2 component. The diffraction pattern was recorded over a 2θ range of 10° – 80° with a step size of 0.02°, and phase identification was carried out using the ICDD database. Thermal stability was assessed using a Perkin Elmer Pyris 1 TGA thermal analyzer, where samples were heated from 30 – 900 °C at a rate of 10 °C/min in a platinum crucible under a nitrogen atmosphere with a gas flow rate of 200 mL/min. Meanwhile, nitrogen sorption analysis was conducted using a Thermo Scientific Surfer Analyzer to determine the surface area and pore size distribution. Prior to measurement, the sample was degassed at −195.8 °C to remove physisorbed species.

Photocatalytic Activity

The photocatalytic prowess of the PMAA-TiO_2 NCs was assessed by subjecting them to the photodegradation of paracetamol, employing a UV lamp with a power output of 6 W and an intensity of 590 μW/cm^2. A 50 mL solution containing 25 ppm of paracetamol was mixed with 0.05 g of PMAA-TiO_2 NCs at room temperature. A magnetic stirrer ensured vigorous swirling at 800 revolutions per minute while the suspension resided in darkness within a UV lamp-equipped box. The system was left in the dark for 1 h to establish adsorption and desorption equilibrium. Subsequently, irradiation commenced, lasting for 3 h, during which 5 mL aliquots were withdrawn at 30 min intervals. The concentration of paracetamol in the samples was determined using a UV–Vis spectrophotometer, and the setup of the photocatalytic reactor is depicted in Figure 1. The degradation percentage was calculated using Equation 1.

$$\text{Degradation percentage (\%)} = \frac{C_o - C}{C_o} \times 100\% \qquad \textbf{(Equation 1)}$$

Where C_o is the initial concentration after 1 h dark reaction, C is the concentration of paracetamol after being treated with UV light irradiation.

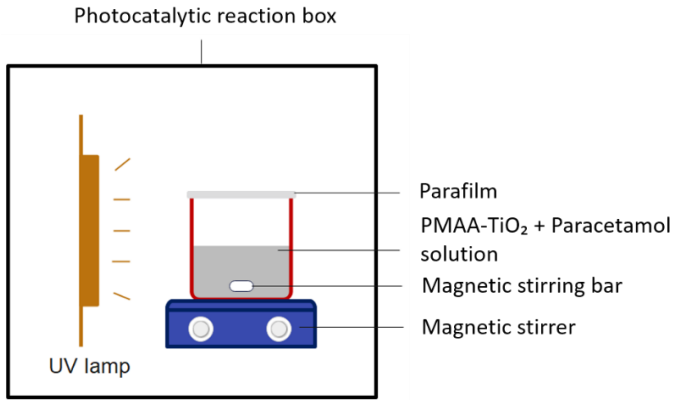

Figure 1. Illustration of the self-built photocatalytic reactor for the photodegradation of paracetamol

pH-Responsiveness Test

The pH-responsiveness was assessed through the photocatalytic degradation of paracetamol in both acidic and basic solutions, with pH levels set at 2 and 11, respectively, under UV light irradiation. The paracetamol solution, derived by diluting 0.25 g of paracetamol in 1 L of distilled water, underwent specific adjustments. For the pH 2 solution, 25 mL was transferred to a flask, and 0.05 M HCl was incrementally added until reaching the desired pH. Similarly, for the pH 11 solution, 0.05 M NaOH was introduced to elevate the pH [29]. The photocatalytic testing occurred within a dark box with a UV lamp. Before initiating the reaction, the mixture was allowed to equilibrate in the dark for 1 h at room temperature with stirring to establish adsorption equilibrium. The actual test spanned 3 h, during which 5 mL of the paracetamol solution was extracted post-reaction. The concentration of paracetamol was determined using a UV–vis spectrophotometer, and the photodegradation efficiency was quantified using Equation 1.

Results and Discussion

This study investigates the physicochemical properties and photocatalytic performance of pH-responsive PMAA-TiO_2 NCs synthesized via free radical polymerization. The structural, thermal, and optical properties of the nanocomposites were first examined to confirm successful incorporation of PMAA and TiO_2. Key features such as functional group presence, crystallinity, and thermal stability varied with TiO_2 and CL content. The photocatalytic activity was then evaluated through paracetamol degradation under UV light.

Functional Groups and Chemical Bonds Analysis by FTIR

The identification of functional groups in both TiO_2 and the prepared PMAA-TiO_2 NCs was accomplished through FTIR spectroscopy. The FTIR spectra of TiO_2 and the synthesized PMAA-TiO_2 NCs are illustrated in Figure 2(A). Commercial TiO_2 exhibits a broad absorption spectrum ranging from 500 cm^{-1} to 1000 cm^{-1}, affirming the presence of Ti-O-Ti bonds [30]. The absorption band at 3418 cm^{-1} corresponds to the stretching vibrations of the O-H group absorbed on the TiO_2 surface [31]. Additionally, the existence of the Ti-OH group is corroborated by the peak at 1626.3 cm^{-1}, signifying water adsorption on the surface of TiO_2 [32].

The FTIR spectra of the synthesized PMAA-TiO_2 NCs reveal distinctive features, including an absorption band at 3442 cm^{-1}, aligning with the absorption band characteristic of TiO_2. This observation signifies the presence of the O-H group adsorbed on the TiO_2 surface [33]. Notably, all the synthesized PMAA-TiO_2 NCs display a prominent peak at 1710 cm^{-1}, attributed to the stretching vibrations of the C=O group originating from PMAA [34]. However, there is an overlap with the peak at 1626.3 cm^{-1} resulting from the bending of the O-H group. The absorption peaks at 2994 cm^{-1} and 2951 cm^{-1} are assigned to the stretching vibrations of methyl and methylene bonds, respectively [35]. This comprehensive data strongly indicates the successful formation of a PMAA layer on the TiO_2 surface.

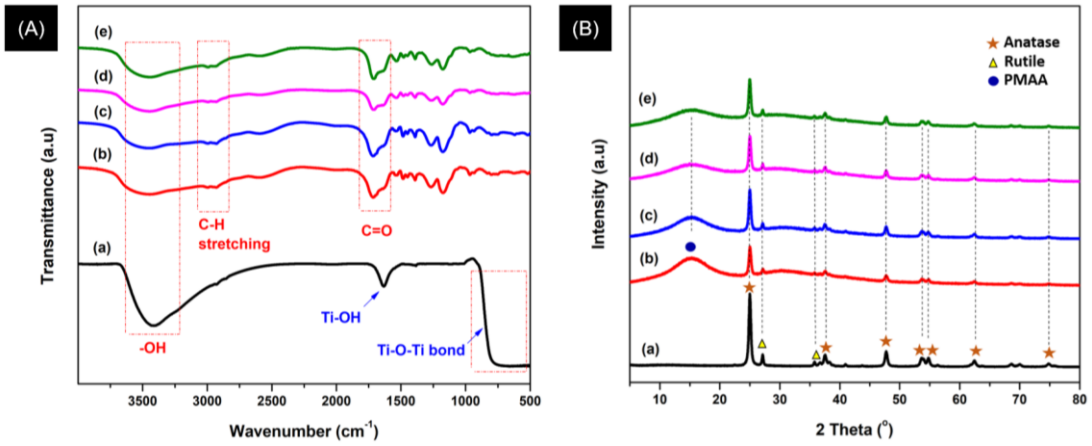

Figure 2. (A) FTIR spectra and (B) XRD patterns of (a) commercial TiO_2, (b) PMAA-TiO_2-0.2, (c) PMAA-TiO_2-0.4, (d) PMAA-TiO_2-0.5CL, and (e) PMAA-TiO_2-0.7CL.

Crystalline Phase Analysis

Figure 2(B) illustrates the X-ray diffraction patterns of the PMAA-TiO_2 NCs. The diffraction peaks of commercial TiO_2, identified at 2θ values of 24.98°, 37.50°, 47.71°, 53.59°, 54.72°, 62.38°, and 74.74°, precisely correspond to the (101), (004), (200), (105), (201), (204), and (215) crystalline planes of anatase TiO_2, respectively. These values align seamlessly with the anatase TiO_2's database, as cataloged in the Joint Committee on Powder Diffraction records (JCPDS 01-075-2553). In addition to the anatase phase, the rutile phase is also detected in the PMAA-TiO_2 NCs. The diffraction peaks manifest at 27.12° and 35.75°, aligning precisely with the (110) and (101) crystalline phases of rutile TiO_2. This alignment is consistent with the ICDD 01-076-1941 database.

The XRD patterns from all PMAA-TiO_2 NCs display peaks identical to those observed in commercial TiO_2. Additionally, the emergence of a distinctive bump at 2θ = 15.12° indicates the presence of the amorphous phase of PMAA. This broad peak strongly suggests the existence of short-range order within the PMAA material, providing valuable insights into its structural characteristics [36]. However, the prevalence of the crystalline phase of TiO_2 within the PMAA matrix has been observed to increase proportionally with the amount of TiO_2 added. The observed increase in diffraction intensity correlates with the augmented presence of TiO_2, attributed to the rise in diffraction centers, while the crystal structure of TiO_2 remains unaltered [28]. This phenomenon is attributed to the additional crosslinks between the TiO_2 and PMAA chains.

The widening of the peak at 2θ = 15.12°, corresponding to the amorphous phase of PMAA, expands in tandem with the number of crosslinkers. As the crosslinker concentration increases within the PMAA matrix, there is a corresponding augmentation in polymer density, leading to an elevation in the number of diffraction centers [37]. Consequently, the increased breadth of the peak indicates a heightened amorphous nature of PMAA. Based on the XRD results, it can be concluded that the successful incorporation of PMAA onto the TiO_2 surface has been achieved without disrupting the inherent crystal structure of TiO_2.

Surface Morphology Analysis

The morphological characteristics and the particle size distribution histogram of the commercial TiO_2 and the synthesized PMAA-TiO_2 NCs are shown in Figure 3. From the FESEM images, it can be seen that the particles of commercial TiO_2 exhibit small sizes and nearly spherical shapes, with some noticeable agglomerations. This agglomeration phenomenon is common in TiO_2, owing to its high surface area to volume ratio, leading to inherent mutual attraction between nanoparticles through van der Waals forces [38]. Upon the addition of PMAA to TiO_2, the images reveal a surface with increased roughness, likely attributable to the presence of PMAA. Interestingly, as the amount of TiO_2 increases, the visibility of PMAA's surface diminishes. This observation suggests a correlation between the concentration of TiO_2 and the visibility of the PMAA layer, hinting at a potential influence on the composite's morphological features.

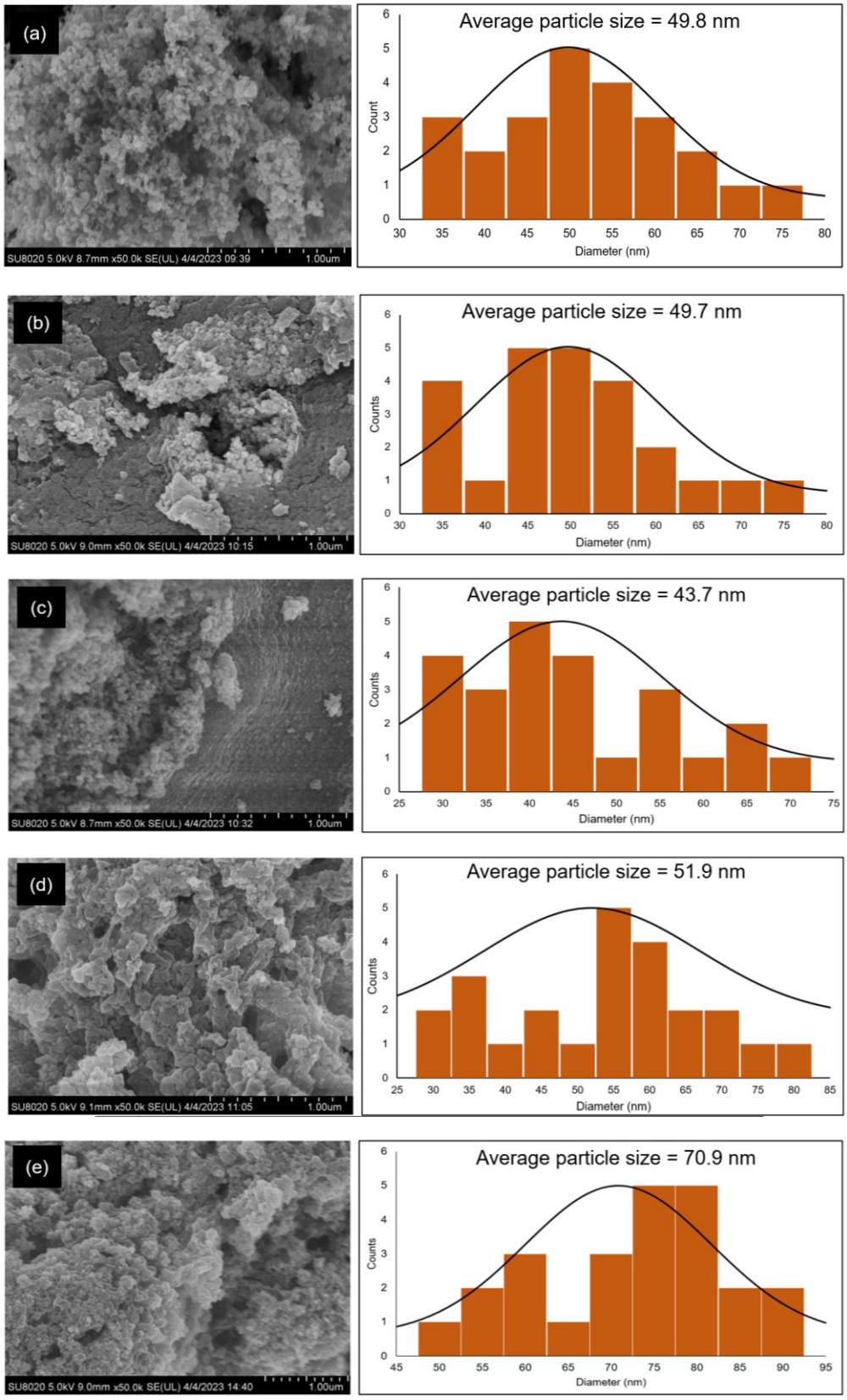

Figure 3. FESEM images and size distribution histogram of (a) commercial TiO_2, (b) PMAA-TiO_2-0.2, (c) PMAA-TiO_2-0.4, (d) PMAA-TiO_2-0.5CL, and (e) PMAA-TiO_2-0.7CL

Furthermore, the augmentation in crosslinker concentration unveils a compact layer structure of PMAA. PMAA establishes a resilient connection within the crosslinking network, effectively linking the polymer chain [39]. However, the observed agglomeration of TiO_2 becomes more pronounced with the escalation of TiO_2's particle size. This phenomenon is likely attributed to the inclination of TiO_2 to minimize its contact surface with PMAA [40].

With regards to the particle size, the average size of TiO_2 nanoparticles in PMAA-TiO_2-0.4 was slightly smaller than in PMAA-TiO_2-0.2, suggesting a significant reduction in the agglomeration of TiO_2 nanoparticles. This reduction is likely attributed to the robust connection between PMAA and TiO_2, effectively impeding TiO_2 agglomeration [41]. However, PMAA-TiO_2-0.7CL exhibits the largest particle size among all the prepared photocatalysts. This is likely induced by the tendency of TiO_2 nanoparticles to minimize their contact surface with PMAA due to the poor compatibility between the crosslinker and TiO_2 [42]. Consequently, an increase in TiO_2 particle agglomeration may have contributed to the observed decrease in particle size.

The energy dispersive X-ray (EDX) analysis was conducted to examine the elemental distribution of the synthesized samples and confirm the successful formation of PMAA-TiO_2 NCs. EDX analysis data are depicted in Figure 4. The synthesized materials are primarily composed of titanium (Ti), oxygen (O), carbon (C), and nitrogen (N). All samples show C species with the highest percentage compared to Ti, N, and O, derived from the polymer chain of PMAA. The percentage of Ti, O, and N species also varied between samples as different amounts of TiO_2 and CL were used. The high atomic percentage of Ti (9.3%) and O (17.5%) in PMAA-TiO_2-0.4 compared with PMAA-TiO_2-0.2 is significant with the amount of TiO_2 added into the polymer matrices. The high atomic percentage of N (5.0%) in PMAA -TiO_2-0.7CL compared with PMAA -TiO_2-0.5CL is significant with the amount of CL added into the polymer matrices. Ti, O, C, and N elements with no other elements confirm that no impurities are present in the sample, which is highly suitable for photocatalytic application [43, 44].

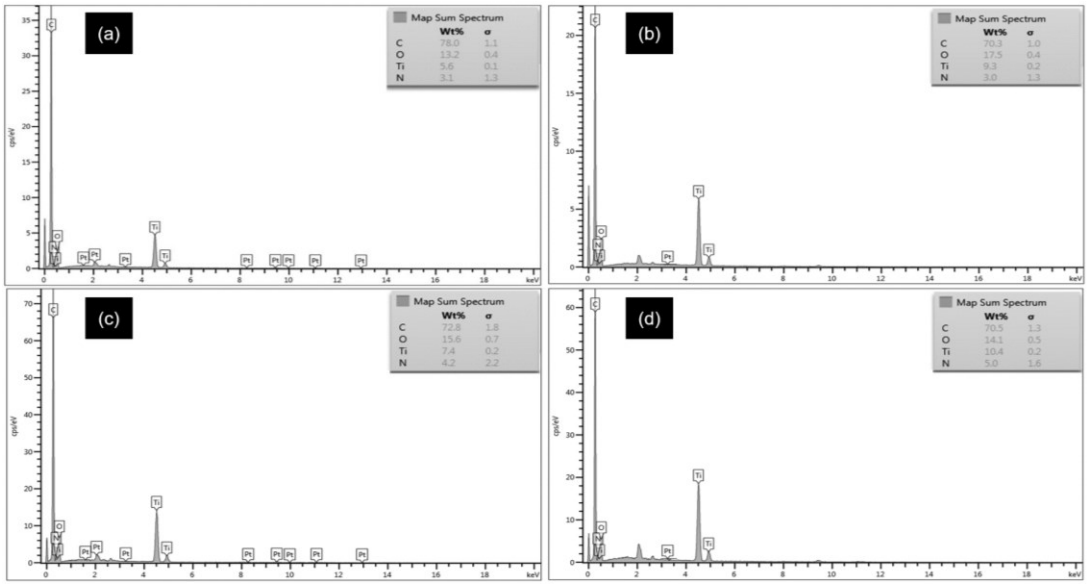

Figure 4. EDX spectra of (a) PMAA-TiO_2-0.2, (b) PMAA-TiO_2-0.4, (c) PMAA-TiO_2-0.5CL, and (d) PMAA-TiO_2-0.7CL.

Optical Properties of PMAA-TiO_2 NCs

Figure 5(A) displays the absorption spectra of commercial TiO_2 and all the prepared PMAA-TiO_2 NCs. Commercial TiO_2 exhibits a greater wavelength in comparison to other synthesized photocatalysts. The addition of the PMAA matrix resulted in a significant shift of the wavelength towards shorter wavelengths, corresponding to the occurrence of blue shift absorption. Kulkarni *et al.* [45] reported that the observed phenomenon could be attributed to the relatively reduced dimensions of the NCs compared to those of commercially available TiO_2.

PMAA-TiO_2-0.4 NCs show higher absorption wavelengths than PMAA-TiO_2-0.2 NCs. As the amount of TiO_2 in PMAA-TiO_2 NCs increases, the absorption edge shifts towards longer wavelengths. According

to Al-Baradi *et al*. [28], this phenomenon can be attributed to the augmentation in the size of the particles. The observed change in position is ascribed to the increase of TiO_2 NPs size during the polymerization process of the PMAA network.

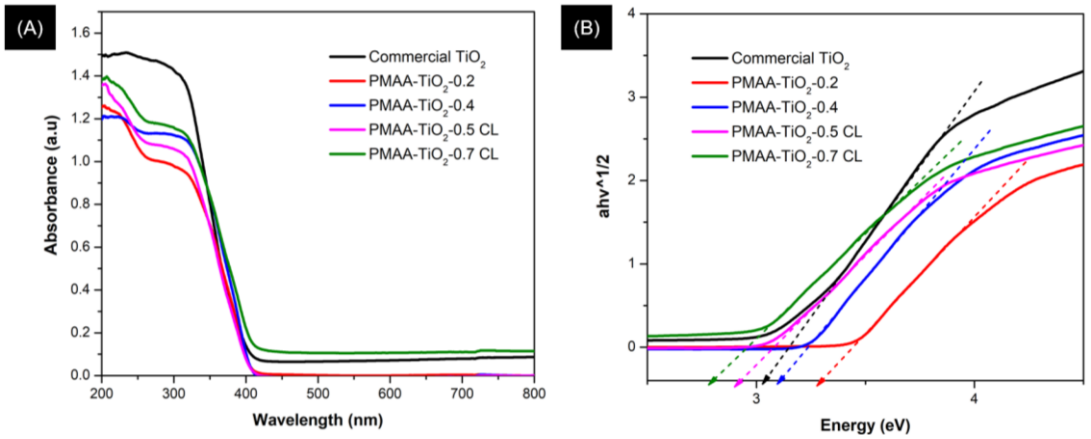

Figure 5. (A) Absorption spectra and (B) Tauc plot of the photocatalysts obtained by UV-vis-NIR spectroscopy

Meanwhile, the absorption wavelength of PMAA-TiO_2-0.5CL NCs and PMAA-TiO_2-0.7CL NCs shifts towards shorter wavelengths than PMAA-TiO_2-0.4 NCs. The increase in crosslinker concentration within PMAA-TiO_2 NCs reduces the absorption edge towards lower wavelengths, ultimately resulting in a blue shift. This observed phenomenon can be attributed to the robust intermolecular connections between the polymer matrix and TiO_2, leading to a shorter bond length and a concurrent reduction in particle dimensions [46]. Consequently, the phenomenon of blue shift absorption is evident.

The evaluation of the photocatalysts' bandgap energy (E_g) involved the analysis of their UV-vis-NIR absorption spectra. The Tauc plot method was employed, plotting $(\alpha hv)^{1/2}$ against energy (hv). The photocatalysts' E_g was determined by linear extrapolation on the plot, as illustrated in Figure 5(B), utilizing the x-intercept value. The E_g value for commercial TiO_2 is 3.2 eV, indicative of the anatase phase of TiO_2 [47]. The augmentation of TiO_2 content in PMAA-TiO_2 leads to a decrease in the E_g value. PMAA-TiO_2-0.2 exhibited an E_g of 3.25 eV, while PMAA-TiO_2-0.4 showed a reduced E_g of 3.07 eV. This reduction in E_g within the PMAA matrix as TiO_2 content increases can be attributed to overlapping localized states originating from TiO_2 aggregates [48].

Moreover, the E_g values further decreased with the addition of crosslinkers, as seen in PMAA-TiO_2-0.5CL (2.90 eV) and PMAA-TiO_2-0.7CL (2.77 eV). This decrease is explained by the introduction of crosslinkers, which increases the number of atomic orbitals available for overlapping, leading to more bonding and antibonding molecular orbitals. According to Santos *et al.* [49], the introduction of crosslinkers results in elevated atomic quantities and an increased number of atomic orbitals available for overlapping. Consequently, the increase in bonding and antibonding molecular orbitals leads to a decrease in E_g. In addition, the reduction in E_g suggests the potential for the photocatalyst to exhibit activity under visible light irradiation, although this aspect was not explicitly examined in the study.

In addition, previous studies have highlighted a close relationship between E_g and surface area. Kanjal *et al.* [50] reported that materials with higher surface area typically provide more defect sites and oxygen vacancies, which can contribute to E_g narrowing and enhanced light absorption. Conversely, a reduction in surface area has been associated with limited defect formation and suppressed charge carrier mobility, thereby restricting photocatalytic efficiency [51]. This indicates that the E_g changes observed in this work are not only governed by TiO_2 aggregation and crosslinking effects but may also be correlated with variations in surface area, together influencing the overall photocatalytic performance of PMAA-TiO_2 NCs.

Thermal Analysis

The thermal stability of PMAA-TiO_2 NCs and commercial TiO_2 was determined by the TGA method. The decomposition rate of PMAA-TiO_2 NCs was evaluated by analyzing the mass loss corresponding to each stage of decomposition based on the TGA curve. The TGA-DTA curves of the synthesized PMAA-TiO_2 NCs are presented in Figure 6.

The thermogram obtained for all the synthesized PMAA-TiO_2 NCs exhibits three distinct decomposition stages. As Gao *et al.* [52] outlined, the initial decomposition stage corresponds to mass reduction attributed to the evaporation of water molecules within the sample. The second stage involves a decrease in mass resulting from the decarboxylation of a portion of the –COOH groups, generating CO_2 [53]. The final stage encompasses the thermal decomposition of the polymer [54]. The third stage of the thermal decomposition of PMAA-TiO_2-0.2 NCs occurring within a temperature range of 320.0 – 532.4 °C, manifests polymer degradation with a weight loss of 59.14% from an initial mass of 11.98 mg. Beyond 532.4 °C, complete polymer decomposition is achieved, with no significant thermal activity observed. The residue's stability under heat treatment confirms its identification as TiO_2 [55].

In the case of the PMAA-TiO_2-0.4 NCs, polymer degradation commences within the temperature range of 340.0 – 547.5 °C, resulting in a weight loss of 56.70% from an initial mass of 11.2 mg. The degradation of the polymer occurs at a temperature slightly higher than observed in other formulations and is influenced by the quantity of TiO_2 within the sample. The increasing amount of TiO_2 imparts higher thermal stability to the sample, attributable to the inherent thermal stability of TiO_2 within the analyzed temperature range [56]. On the other hand, the PMAA-TiO_2-0.4 NCs exhibit the highest thermal stability among all samples due to the robust interaction between TiO_2 and the PMAA chains [57]. Consequently, the polymer initiates degradation at an elevated temperature of 340.0 °C, highlighting the substantial impact of the strong interplay between TiO_2 and PMAA on enhancing thermal stability.

Apart from that, the thermal behavior of PMAA-TiO_2-0.5CL NCs is characterized by polymer degradation initiating within a temperature range of 280.0 – 525.6 °C, resulting in a weight loss of 40.63% from the initial mass of 13.4 mg. Notably, this degradation onset occurs at marginally lower temperatures than PMAA-TiO_2-0.4 NCs. The heightened presence of crosslinkers contributes to enhanced thermal stability, given the increased cross-links within the particles. However, intriguingly, PMAA-TiO_2-0.5CL NCs exhibit less thermal stability, potentially attributable to their smaller particle sizes and larger specific surface area. This unique characteristic facilitates significant contact and diffusion of nitrogen gas, ultimately leading to degradation at a lower temperature for PMAA-TiO_2-0.5CL NCs.

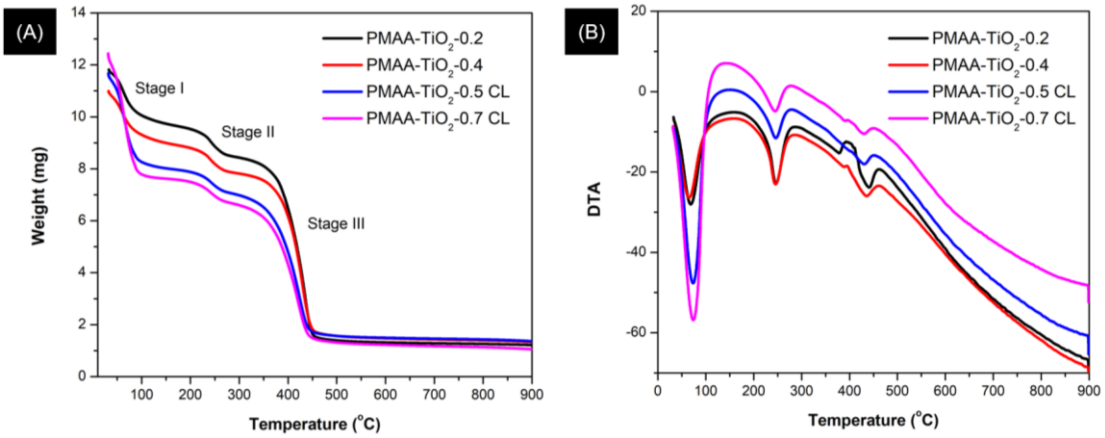

Figure 6. (A) TGA and (B) DTA curves of the synthesized PMAA-TiO_2 NCs

The thermal degradation behavior of PMAA-TiO_2-0.7CL unfolds in a temperature range spanning from 290.0 – 510.5 °C, resulting in a weight loss of 41.56% from the initial mass of 12.9 mg. Significantly, the onset of polymer degradation occurs at a slightly elevated temperature compared to PMAA-TiO_2-0.5CL. This variation in degradation temperature is likely influenced by the concentration of crosslinkers embedded in the sample. The augmented presence of crosslinkers within the PMAA matrix corresponds to an increased polymer density, facilitating robust linkages among the crosslinkers, PMAA, and TiO_2. This intricate network of interactions substantially enhances the stability of PMAA at elevated temperatures. Consequently, a discernible trend emerges, revealing that the temperature at which polymer decomposition takes place experiences a subtle increment with the greater concentration of crosslinkers present in the PMAA-TiO_2-0.7CL sample.

Photocatalytic Activity

The determination of the photocatalytic activity of the synthesized photocatalysts is an essential part of the photodegradation study. This study utilized paracetamol as the representative organic contaminant

to evaluate the photocatalytic efficacy of commercial TiO_2, PMAA-TiO_2-0.2, PMAA-TiO_2-0.4, PMAA-TiO_2-0.5CL, and PMAA-TiO_2-0.7CL under UV light irradiation. Variations in the percentage of photodegradation of paracetamol were anticipated in the presence of PMAA-TiO_2, contingent upon the amount of TiO_2 and crosslinkers utilized.

Figure 7 illustrates the degradation percentage of paracetamol using the synthesized photocatalysts after 3 h exposure to UV light irradiation. The photocatalytic reaction was carried out directly without adjusting the solution's pH; throughout the photocatalytic reaction, the recorded pH remained near neutral (pH 6 – 7). In the absence of photocatalysts (photolysis), there was minimal degradation (5.94%), highlighting the necessity of photocatalysts to significantly enhance paracetamol degradation under UV light. Among the PMAA-TiO_2 photocatalysts with varying TiO_2 concentrations, PMAA-TiO_2-0.4 demonstrated the highest degradation at 32.48%, while PMAA-TiO_2-0.2 showed the lowest at 18.78%.

The relationship between the TiO_2 quantity, PMAA-TiO_2 NCs, and their photocatalytic efficiency is evident. The higher the amount of TiO_2 in PMAA-TiO_2 NCs, the higher the photocatalytic efficiency of the photocatalyst. The increased TiO_2 concentration leads to an enhanced surface-volume ratio, improving light absorption and the separation efficiency of photoexcited charge carriers [58]. Consequently, the enhanced separation efficiency of photoexcited charge carriers will increase surface photoactivity and improve the photocatalytic activity of PMAA-TiO_2 NCs.

Similarly, varying crosslinker concentrations in PMAA-TiO_2 NCs also significantly affect photocatalytic efficiency. PMAA-TiO_2-0.7CL demonstrated the highest degradation percentage at 46.22%, while PMAA-TiO_2-0.5CL recorded the lowest at 25.74%. A higher concentration of crosslinkers enhances the structural integrity of the PMAA-TiO_2 NCs and facilitates the formation of a robust and interconnected network [59]. This network improves the dispersion of TiO_2 within the PMAA matrix, ensuring better accessibility of active sites for photocatalytic reactions [60], further enhancing photocatalytic efficiency.

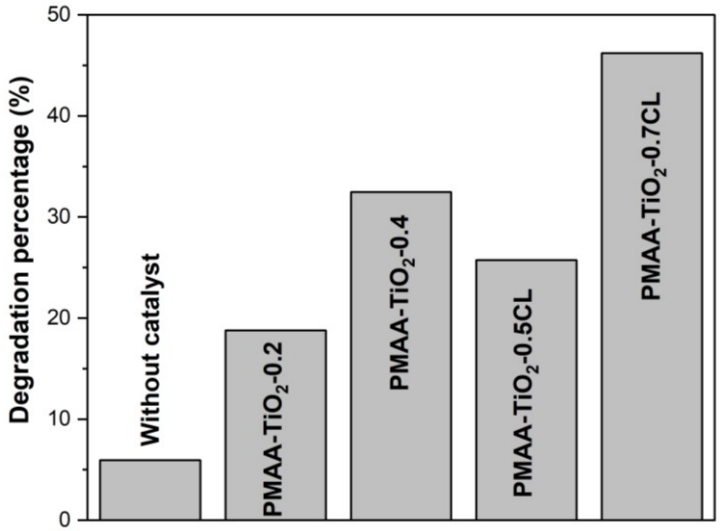

Figure 7. Degradation percentage of paracetamol under UV light irradiation in the presence of different photocatalysts. Experimental conditions: addition of photocatalyst (0.05 g) in paracetamol (25 ppm) at near-neutral pH (6 – 7) and reaction time of 3 h

Figure 8 directly compares the photocatalytic performance of commercial TiO_2 and PMAA-TiO_2-0.7CL in the degradation of paracetamol under UV light irradiation. Commercial TiO_2 achieved an outstanding 99.01% degradation after 3 h, while PMAA-TiO_2-0.7CL exhibited a relatively lower, yet significant, degradation percentage of 46.22%. This comparison highlights the superior performance of commercial TiO_2 in photocatalysis due to its established efficiency under UV light. However, PMAA-TiO_2-0.7CL still displays promising performance, especially considering the limitations imposed by the polymer matrix surrounding the TiO_2 nanoparticles.

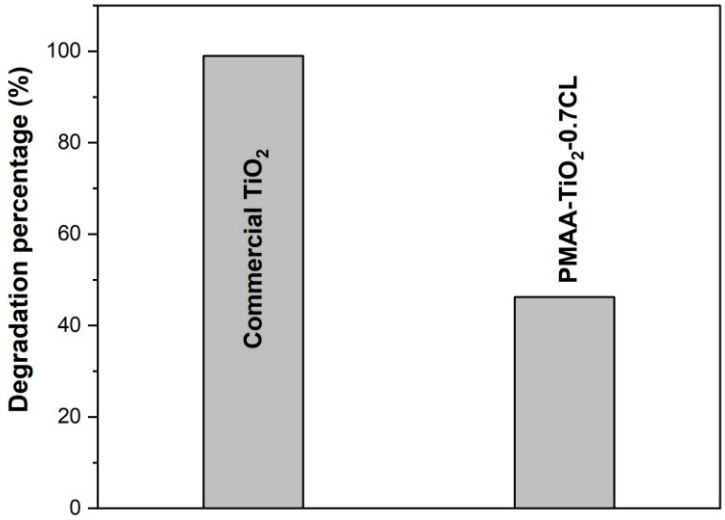

Figure 8. Comparison of the degradation percentage of paracetamol under UV light irradiation in the presence of commercial TiO_2 and PMAA-TiO_2-0.7CL. Experimental conditions: addition of photocatalyst (0.05 g) in paracetamol (25 ppm) at near-neutral pH (6 – 7) and reaction time of 3 h

To better contextualize these results, a comparison with previous studies conducted under nearly similar conditions is presented in Table 2. Table 2 summarizes representative studies on the photocatalytic degradation of paracetamol using TiO_2-based photocatalysts under UV irradiation. Conventional modifications such as TiO_2-cellulose paper (TiO_2-CP) [61], TiO_2-graphite (TiO_2-G) [62], and TiO_2-activated carbon (TiO_2-AC) [63] achieved high degradation efficiencies (> 90%), while other systems such as TiO_2-carbon nitrogen (TiO_2-C-N) [64] and TiO_2-nickel copper (TiO_2-NiCu) [65] demonstrated moderate performance depending on paracetamol concentration and irradiation time. In this work, the PMAA-TiO_2-0.7CL NCs achieved 46.2% degradation after 3 h at 25 ppm, which is lower than conventional TiO_2-based modifications. However, unlike those systems, the PMAA-TiO_2 NCs provide pH-responsive behavior and tunable optical properties, representing a distinct approach to developing smart photocatalysts capable of adapting to environmental conditions, as will be highlighted later in the discussion on their functional performance.

Table 2. Photocatalytic degradation of paracetamol using TiO_2-based photocatalysts under UV irradiation.

Photocatalyst	Paracetamol (ppm)	Light source	Irradiation time (h)	Degradation (%)	Ref.
Commercial TiO_2	25	UV	3	99.00	Present study
PMAA-TiO_2-0.7CL	25	UV	3	46.20	Present study
TiO_2-CP	25	UV	4	98.00	[61]
TiO_2-G	25	UV	3	100.00	[62]
TiO_2-AC	25	UV	3	90.00	[63]
TiO_2-C-N	4	UV	2	69.31	[64]
TiO_2-NiCu	10	UV	3	80.00	[65]

Nitrogen sorption analysis was conducted to further understand the disparity in photocatalytic performance between these two materials by exploring their structural characteristics, which directly influence photocatalytic activity. The adsorption-desorption isotherms and pore size distributions of both materials were analyzed and are depicted in Figure 9. The commercial TiO_2 exhibited a well-defined Type IV isotherm with pores ranging from 3 to 16 nm, indicating a mesoporous material. PMAA-TiO_2-0.7CL also demonstrated a Type IV isotherm but with reduced mesoporosity, as indicated by the shift in pore size distribution towards the 8 – 16 nm range.

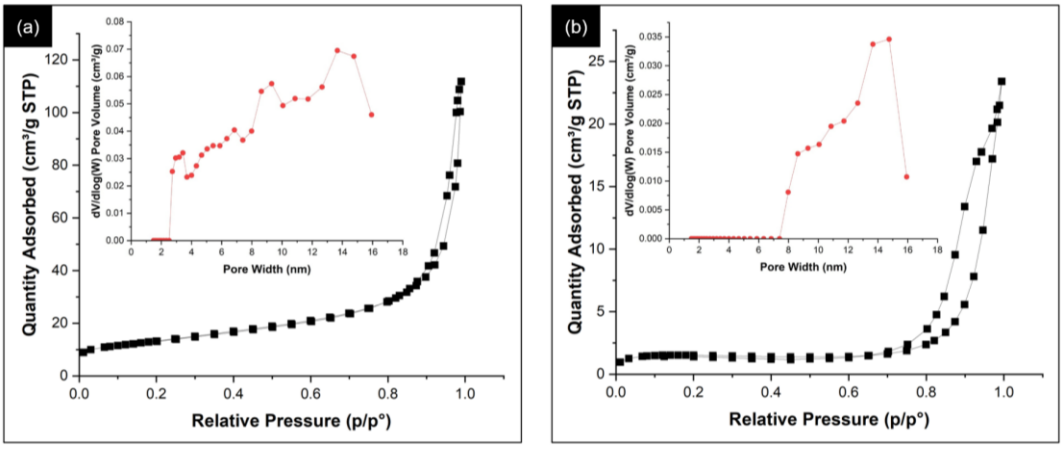

Figure 9. The adsorption-desorption isotherm and pore size distribution of (a) commercial TiO_2 and (b) PMAA-TiO_2-0.7CL

Table 3 presents the BET surface area and pore volume data for both materials. The BET surface area of commercial TiO_2 was determined to be 46.42 m^2/g, with a pore volume of 0.0402 cm^3/g, indicating a high degree of porosity and available surface area for photocatalytic reactions. These characteristics favour photocatalytic activity, as a high surface area provides more active sites for reactions [66]. At the same time, a larger pore volume enhances the diffusion of paracetamol to these active sites, facilitating more efficient degradation.

Table 3. The BET surface area and pore volume of the photocatalysts.

Samples	Surface area (m^2/g)	Pore volume (cm^3/g)
Commercial TiO_2	46.42	0.0402
PMAA-TiO_2-0.7CL	5.93	0.0077

On the other hand, PMAA-TiO_2-0.7CL exhibited a significantly lower BET surface area of 5.93 m^2/g and a pore volume of 0.0077 cm^3/g. This reduction can be attributed to the introduction of crosslinkers, which create a dense polymer network around the TiO_2 nanoparticles [59]. Crosslinkers are chemically reactive agents that establish covalent bonds between polymer chains, resulting in a more rigid and interconnected polymer network. This network effectively fills the pores and reduces their accessibility, limiting the available surface area for photocatalytic reactions [67]. It should be noted that the nitrogen sorption analysis was conducted after the sample was dried. During this process, nitrogen molecules were adsorbed at the surface of the material to determine surface area and porosity. However, it does not account for the material's behavior in a liquid environment. Additionally, nitrogen sorption analysis cannot measure the surface area under varying pH conditions, which would influence the swelling and shrinking of the polymer network. As a result, the lower surface area observed may be due to the limitations of this method, as it does not reflect the polymer's pH-responsive behavior during actual photocatalytic reactions.

Despite the reduced surface area, PMAA-TiO_2-0.7CL demonstrated superior photocatalytic performance compared to the other nanocomposites prepared. This enhancement is primarily due to the improved dispersion of TiO_2 within the polymer matrix, which allows for better light absorption and photoactivity. This strategic enhancement of TiO_2 dispersion compensates for the lower surface area and contributes to the higher degradation efficiency observed.

Although these findings highlight the efficiency of PMAA-TiO_2 NCs, their pH-responsiveness remains untested. Recognizing the potential influence of environmental conditions on photocatalytic performance, the subsequent experiment focuses on pH-responsiveness tests. This strategic approach aims to determine the adaptability and effectiveness of these nanocomposites across a range of pH variations.

pH-responsiveness Test

The pH-responsive test of commercial TiO_2 and the synthesized PMAA-TiO_2 NCs was optimized with

0.4 g of TiO_2 and 0.7 g of crosslinkers. This test involved subjecting paracetamol to photodegradation under varying pH conditions —specifically, at pH 2 under acidic conditions and pH 11 under basic conditions — while exposed to UV light irradiation. Figure 10 visually represents the paracetamol degradation percentage in the presence of commercial TiO_2 and the synthesized PMAA-TiO_2-0.7CL photocatalyst during a 3 h UV light exposure under both basic and acidic conditions. In the presence of commercial TiO_2, the degradation percentages were not significantly different, with slightly higher values under basic conditions (55.75%) compared to acidic conditions (53.45%). This suggests that commercial TiO_2 is not pH-responsive. The slight increase in basic conditions compared to acidic conditions may be attributed to the surface charge, which affects the photocatalytic process. Under alkaline conditions, hydroxyl radicals (•OH) are produced directly from the hydroxide ions (OH^-), which interact with the holes [68]. Therefore, the resulting •OH will be more numerous under alkaline conditions, enhancing the photocatalytic ability. In contrast, in acidic conditions, an excess of OH exists, which interacts with free electrons to form radicals [69]. The formation of these radicals will cause a reaction with •OH, converting them to H_2O. This reduces the amount of •OH, resulting in lower photocatalytic activity under acidic conditions.

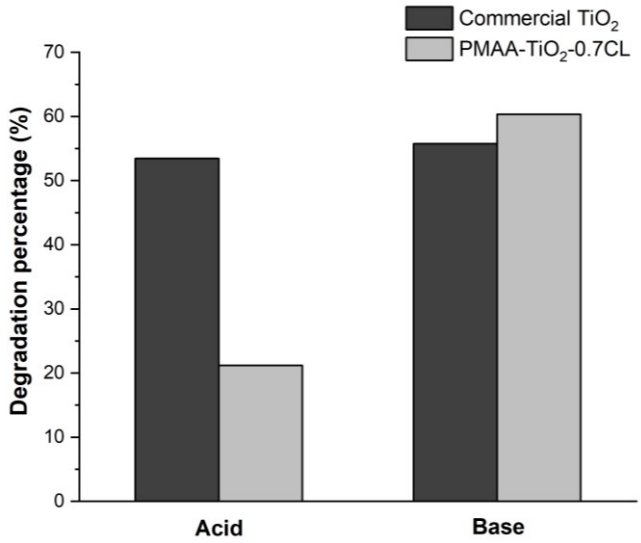

Figure 10. Degradation percentage of paracetamol under UV light irradiation in the presence of commercial TiO_2 and PMAA-TiO_2-0.7CL. Experiment condition: photocatalyst (0.05 g) was added to paracetamol with different pHs; acidic (pH 2, using 0.05 M HCl) and basic (pH 11, using 0.05 M NaOH). Reaction time: 3 h

In contrast, the PMAA-TiO_2-0.7CL photocatalyst exhibited pH-responsive behavior, significantly varying its degradation efficiency across different pH levels. This pH-responsiveness is evident in a higher degradation percentage in basic conditions (60.35%), surpassing its performance in acidic conditions (21.10%), showcasing the pH-responsive nature. PMAA is recognized for its pronounced pH-responsive gating, and the dynamics of PMAA-TiO_2 nanocomposites and the degradation process are contingent on the pH of the solution [29]. PMAA exhibits a pH-responsive mechanism wherein it can undergo either swelling or contraction in response to changes in its surrounding environment [70], as illustrated in Figure 11.

Under UV light irradiation, the PMAA/TiO_2 NCs initiate a photocatalytic process where photons excite electrons in TiO_2, moving them from the valence band (VB) to the conduction band (CB) and generating electron-hole pairs [71]. The PMAA matrix enhances this process by promoting greater charge separation and reducing recombination, improving photocatalytic efficiency. However, the efficiency of this process is highly pH-dependent due to the swelling and shrinking behavior of PMAA. In acidic conditions, the PMAA shrinks as its carboxylic groups become protonated, causing the polymer matrix to contract [72]. This compact state limits the exposure of TiO_2 active sites, reducing the diffusion of reactive species and hindering the migration of charge carriers, resulting in lower photocatalytic efficiency for paracetamol degradation.

Significantly, an improvement in the effectiveness of photocatalysis was observed under basic conditions. This observed phenomenon can be attributed to the swelling effect induced by PMAA within PMAA-TiO_2 NCs. Under high pH conditions, the PMAA layer ionized, forming negatively charged carboxylate anions that caused swelling, enhancing the photocatalyst's surface area and active site availability [73]. Electrostatic repulsion between the carboxylic acid (-COOH) groups leads to this swelling, expanding the polymer and significantly increasing the photocatalyst's surface area. This expansion enhances photocatalytic efficacy by providing more active sites [60]. As a result, electron transfer and reactive oxygen species (ROS) generation are promoted [74], contributing to the higher degradation efficiency observed in alkaline conditions. The increased hydrophilicity of the PMAA layer also facilitates better interaction between the photocatalyst and paracetamol [70], optimizing the degradation process. Therefore, the photocatalytic activity increases under alkaline conditions, highlighting the successful incorporation of the pH-responsive feature by modifying TiO_2 with PMAA.

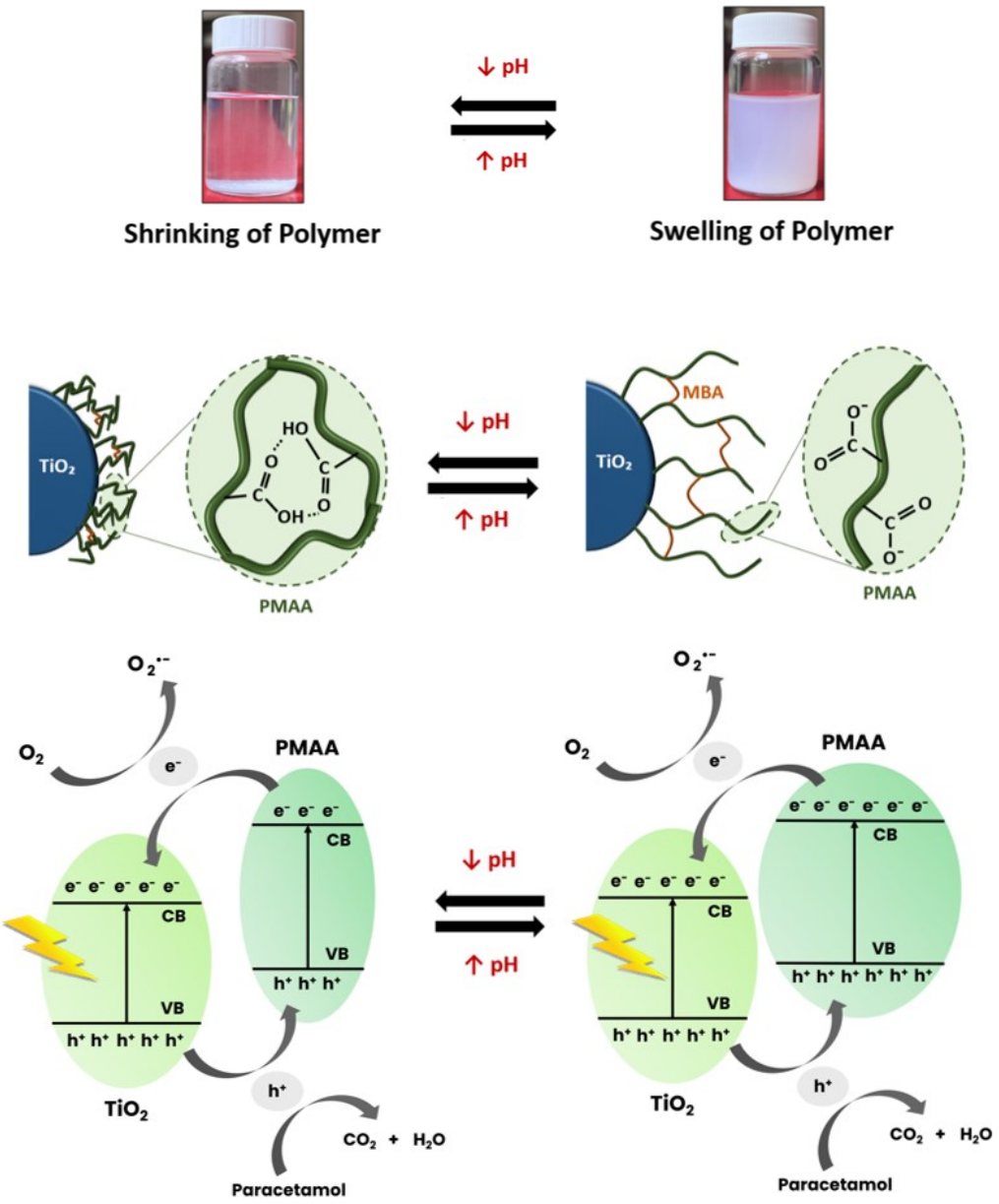

Figure 11. Swelling and shrinking behaviour of PMAA-TiO_2 NCs

Conclusions

This study synthesized a series of PMAA-TiO_2 NCs through free radical polymerization with varying TiO_2 nanoparticles and cross-linkers. The successful incorporation of PMAA into TiO_2 was confirmed by FTIR, FESEM, EDX, XRD, and UV-vis-NIR spectroscopy, revealing no alteration to the anatase phase of TiO_2. Instead, the incorporation of PMAA and cross-linkers significantly influenced the particle size, surface morphology, and thermal stability of the nanocomposites. Among all the prepared samples, PMAA-TiO_2-0.4 NCs exhibited the highest photocatalytic activity due to their higher TiO_2 content, enhancing light absorption and surface photoactivity. Cross-linker variation facilitated a robust network, improving the accessibility of active sites, with PMAA-TiO_2-0.7CL NCs achieving the highest photocatalytic degradation of 46.22% under UV light. In the pH-responsive tests, the commercial TiO_2 showed slightly different degradation percentages under acidic (53.45%) and basic (55.75%) conditions, indicating limited pH responsiveness. Conversely, PMAA-TiO_2-0.7CL NCs demonstrated the highest percentage of paracetamol degradation (60.32%) under UV light in basic conditions. This result is credited to the deprotonation of -COOH groups on PMAA, leading to PMAA swelling and improved photocatalytic efficiency by providing additional active sites. Thus, the synthesized PMAA-TiO_2 NCs in this work showed promising characteristics as pH-responsive photocatalysts.

Conflicts of Interest

The authors declare that there is no conflict of interest regarding the publication of this paper.

Acknowledgments

The authors would like to acknowledge funding provided by Universiti Teknologi Malaysia from Geran Penyelidikan Hi-Tech (F4) (Q.J130000.4654.00Q19) and PDRU Grant Vote No. 07E44.

References

[1] Nagaraj, K., Radha, S., Deepa, C. G., Raja, K., Umapathy, V., Badgujar, N. P., Parekh, N. M., Manimegalai, T., Archana Devi, L., & Uthra, C. (2025). Photocatalytic advancements and applications of titanium dioxide (TiO_2): Progress in biomedical, environmental, and energy sustainability. *Next Research*, *2*(1), 100180.

[2] Piracha, S., Batool, S., Zhang, Y., Miao, Y.-X., Li, G., & Hasan, M. (2025). Unfolding the significance of metal oxides for photocatalytic sustainable water splitting combined with organic pollutants. *Journal of Materials Science*, *60*(13), 5721–5748.

[3] Zeng, K., Cheng, L., Hu, W., & Li, J. (2025). Synthesis, stability, and tribological performance of TiO_2 nanomaterials for advanced applications. *Lubricants*, *13*(2), 56.

[4] Jenima, J., Priya Dharshini, M., Ajin, M. L., Jebeen Moses, J., Retnam, K. P., Arunachalam, K. P., Avudaiappan, S., & Arrue Munoz, R. F. (2024). A comprehensive review of titanium dioxide nanoparticles in cementitious composites. *Heliyon*, *10*(20), e39238.

[5] Anucha, C. B., Altin, I., Bacaksiz, E., & Stathopoulos, V. N. (2022). Titanium dioxide (TiO_2)-based photocatalyst materials activity enhancement for contaminants of emerging concern (CECs) degradation: In the light of modification strategies. *Chemical Engineering Journal Advances*, *10*, 100264.

[6] Chakravorty, A., & Roy, S. (2024). A review of photocatalysis, basic principles, processes, and materials. Sustainable Chemistry for the Environment, *8*, 100155.

[7] Abdelfattah, I., & El-Shamy, A. M. (2024). A comparative study for optimizing photocatalytic activity of TiO_2-based composites with ZrO_2, ZnO, Ta_2O_5, SnO, Fe_2O_3, and CuO additives. *Scientific Reports*, *14*(1), 27175.

[8] Ennami, N., Ait Blal, A., El Fallah, J., Clet, G., Hadjiivanov, K., Maugé, F., & Aboulayt, A. (2025). Mesoporous anatase–brookite TiO_2: Surface acidity and performance in isopropanol catalytic dehydration. *Catalysis Letters*, *155*(9), 290–301.

[9] Khoiriah, K., Putri, R., Ratnawati, R., & Sari, M. (2024). Investigating the effect of hydrogen peroxide on photocatalytic degradation of commercial paracetamol using TiO_2. *Journal of Chemical Technology and Metallurgy*, *59*(3), 539–548.

[10] Akşit, D. A., & Pozan Soylu, G. (2022). Photocatalytic degradation of paracetamol by semiconductor oxides under UV and sunlight illumination. *Turkish Journal of Chemistry*, *46*(5), 1243–1254.

[11] Che Ku Hitam, C. K., & Abdul Jalil, A. (2020). A review on exploration of Fe_2O_3 photocatalyst towards degradation of dyes and organic contaminants. *Journal of Environmental Management, 258,* 110050.

[12] Brillas, E., & Manuel Peralta-Hernández, J. (2023). Removal of paracetamol (acetaminophen) by photocatalysis and photoelectrocatalysis: A critical review. *Separation and Purification Technology, 309,* 122982.

[13] Mohamed, W. A. A., Alhodaib, A., Mousa, H. A., Handal, H. T., Galal, H. R., Abd El-Gawad, H. H., Elsayed, B. A., Labib, A. A., & Abdel-Mottaleb, M. S. A. (2025). Principles, applications and future prospects in

photodegradation systems. *Journal of Photochemistry and Photobiology, 14*(1), 100112.

[14] Patroklou, G., Mohamed, W. A. A., Alhodaib, A., Mousa, H. A., Handal, H. T., Galal, H. R., Abd El-Gawad, H. H., Elsayed, B. A., Labib, A. A., & Abdel-Mottaleb, M. S. A. (2025). pH-responsive hydrogels: Recent advances in pharmaceutical applications. *Polymers, 17*(11), 1451.

[15] Zhou, H., Wang, H., Yue, C., He, L., Li, H., Zhang, H., Yang, S., & Ma, T. (2024). Photocatalytic degradation by TiO_2-conjugated/coordination polymer heterojunction: Preparation, mechanisms, and prospects. *Applied Catalysis B: Environment and Energy, 344,* 123605.

[16] Sabet, M. (2025). Revolutionizing structures: The rise of high-performance composite and nanocomposite polymers. *Polymer Bulletin, 82*(10), 4257–4306.

[17] Infantiya, S. G., Anbuselvi, D., & Vanitha, N. S. (2025). Emerging trends and future developments in smart materials and their applications. In *New Frontiers in Materials Science* (pp. 215–240). Springer.

[18] Nikishau, P., Kozlovskaya, V., & Kharlampieva, E. (2024). Controlled synthesis and pH-sensitive complexation of poly(methacrylic acid) polyampholytes. *Polymer Chemistry, 15*(40), 4151–4163.

[19] Simeonov, M., Yildirim, I., Tzachev, C. T., & Vassileva, E. (2025). Stimuli-responsive hydrogels of poly(methacrylic acid)/poly(N,N-dimethylacrylamide) interpenetrating polymer networks as drug delivery systems for promethazine hydrochloride. *Gels, 11*(4), 240.

[20] Loo, S.-L., Vásquez, L., Athanassiou, A., & Fragouli, D. (2021). Polymeric hydrogels—A promising platform in enhancing water security for a sustainable future. *Advanced Materials Interfaces, 8*(24), 2100580.

[21] Jin, S., Shaaban, E., Bamonte, S., Cintron, D., Shuster, S., Zhang, L., Li, G., & He, J. (2021). Surface basicity of Metal@TiO_2 to enhance photocatalytic efficiency for CO_2 reduction. *ACS Applied Materials & Interfaces, 13*(32), 38595–38603.

[22] Spasojević, L., Ivanišević, I., & Dutour Sikirić, M. (2025). Stability and application of TiO_2 nanomaterials in aqueous suspensions: A review. *RSC Advances, 15*(27), 21341–21368.

[23] Wang, M., Liu, L., Cui, Y., Geng, H., Zhao, H., Liang, B., & Yang, J. (2019). Effects of specific surface area and oxygen vacancy on the photocatalytic properties of mesoporous F-doped SnO_2 nanoparticles prepared by hydrothermal method. *Journal of Materials Science: Materials in Electronics, 30*(17), 16110–16123.

[24] Orozco-Noriega, V. A., & Cortez-Lemus, N. A. (2025). Synthetic strategies for the preparation of hydrogels using star-shaped polymers. *Polymer Bulletin.*

[25] Elvir-Lazo, O. L., Woldemariam, Z., Romero-Navarro, A. L., Yumul, R., & White, P. F. (2025). Role of acetaminophen in chronic pain management: Benefits, risks, and considerations. *Journal of Surgery and Research, 8*(2), 176–181.

[26] Tony, A. A., Tony, E. A. E., Ali, S. B., Ezzeldin, A. M., & Mahmoud, A. A. (2020). COVID-19-associated sleep disorders: A case report. *Neurobiology of Sleep and Circadian Rhythms, 9,* 100057.

[27] Morante, N., Monzillo, K., Vaiano, V., Kadirova, Z. C., & Sannino, D. (2025). Synthesis and characterization of a novel sol–gel-derived Ni-doped TiO_2 photocatalyst for rapid visible light-driven mineralization of paracetamol. *Nanomaterials, 15*(5), 1005.

[28] Al-Baradi, A. M., Al-Shehri, S. F., Badawi, A., Merazga, A., & Atta, A. A. (2018). A study of optical, mechanical and electrical properties of poly(methacrylic acid)/TiO_2 nanocomposite. *Results in Physics, 9,* 879–885.

[29] Wardhani, S., Purwonugroho, D., Fitri, C. W., & Prananto, Y. P. (2018). Effect of pH and irradiation time on TiO_2-chitosan activity for phenol photodegradation. *IOP Conference Series: Materials Science and Engineering, 299,* 012083.

[30] Jadhav, V., Patil, M., Pardeshi, S., Suryavanshi, H., & Bhagare, A. (2025). Green synthesis of Ag@ TiO_2 nanomaterials using *Achyranthes aspera* leaf extract for sustainable photocatalytic degradation of dyes. *Discover Applied Sciences, 7*(7), 732.

[31] Algreiby, A. A., Alnafisah, A. S., Alrasheedi, M., Alresheedi, T. M., Taha, K. K., & Modwi, A. (2025). Harnessing C@Zn@TiO_2 nanocomposites for cadmium adsorption in aquatic media. *International Journal of Environmental Analytical Chemistry.*

[32] Šolić, M., Nikić, J., Kulić Mandić, A., Apostolović, T., Watson, M., Kragulj Isakovski, M., & Maletić, S. (2025). Unraveling adsorption mechanisms and potential of titanium dioxide for arsenic and heavy metal removal from water sources. *Processes, 13*(6), 1618.

[33] Ibrahim, A. I., & Vohra, M. S. (2025). Novel TiO_2@Mg/Fe-LDH for photocatalysis and adsorption of selenium species from wastewater: RSM & ANN/ML modeling. *Next Materials, 8,* 100766.

[34] Kocijan, M., Ćurković, L., Vengust, D., Radošević, T., Shvalya, V., Gonçalves, G., & Podlogar, M. (2023). Synergistic remediation of organic dye by titanium dioxide/reduced graphene oxide nanocomposite. *Molecules, 28*(21), 7326.

[35] Zhang, Y., Gu, W., Zhao, J., & Qin, Z. (2017). A facile, efficient and "green" route to pH-responsive crosslinked poly(methacrylic acid) nanoparticles. *Colloids and Surfaces A: Physicochemical and Engineering Aspects, 531,* 1–8.

[36] Kuleyin, H., & Gümrük, R. (2025). The effect of poly(methyl methacrylate) content on chemical, thermomechanical, mechanical, and fatigue life characteristics of ternary PC/ABS/PMMA blends. *Polymers, 17*(14), 1905.

[37] Mejenom, A. A., Hafiza, M. N., & Isa, M. I. N. (2018). X-ray diffraction and infrared spectroscopic analysis of solid biopolymer electrolytes based on dual blend carboxymethyl cellulose-chitosan doped with ammonium bromide. *ASM Science Journal Special Issue 2018,* 2018, 90–96.

[38] Endres, S. C., Ciacchi, L. C., & Mädler, L. (2021). A review of contact force models between nanoparticles in agglomerates, aggregates, and films. *Journal of Aerosol Science, 153,* 105719.

[39] Chen, J., Garcia, E. S., & Zimmerman, S. C. (2020). Intramolecularly cross-linked polymers: From structure to function with applications as artificial antibodies and artificial enzymes. *Accounts of Chemical Research, 53*(6), 1244–1256.

[40] Liza, T. Z., Tusher, M. M. H., Anwar, F., Monika, M. F., Amin, K. F., & Asrafuzzaman, F. N. U. (2024). Effect of Ag-doping on morphology, structure, band gap and photocatalytic activity of bio-mediated TiO_2 nanoparticles. *Results in Materials, 22,* 100559.

[41] Jerczynski, K., Lipinska, M., Raj, W., Šlouf, M., Halagan, K., Kozanecki, M., Grobelny, J., Matyjaszewski, K., & Pietrasik, J. (2022). Effect of hybrid TiO_2 nanoparticles with controlled morphology on rheological properties of poly(styrene-co-acrylonitrile) nanocomposites. *Materials Today Chemistry, 26,* 101189.

[42] Zeljko, M., Ocelić Bulatović, V., Špada, V., & Blagojević, S. L. (2021). Environmentally friendly UV-protective polyacrylate/TiO_2 nanocoatings. *Polymers, 13*(16), 2609.

[43] Sadikin, S. N., Ridwan, J., Umar, M. I. A., Raub, A. A. M., Yunas, J., Hamzah, A. A., Dahlan, D., Rahman, M. Y. A., & Umar, A. A. (2023). Photocatalytic activity and stability properties of porous TiO_2 film as photocatalyst for methylene blue and methylene orange degradation. *International Journal of Electrochemical Science, 18*(9), 100284.

[44] Ba-Abbad, M. M., Kadhum, A. A. H., Mohamad, A. B., Takriff, M. S., & Sopian, K. (2012). Synthesis and catalytic activity of TiO_2 nanoparticles for photochemical oxidation of concentrated chlorophenols under direct solar radiation. *International Journal of Electrochemical Science, 7*(6), 4871–4888.

[45] Kulkarni, H., Mladenov, N., & Datta, S. (2019). Effects of acidification on the optical properties of dissolved organic matter from high and low arsenic groundwater and surface water. *Science of the Total Environment, 653,* 1326–1332.

[46] Zhao, H., Zhang, Q., Wen, X., Wang, G., Gong, X., & Shi, X. (2021). Dual covalent cross-linking networks in polynorbornene: Comparison of shape memory performance. *Materials, 14*(12), 3249.

[47] Suhaimi, N. H. S., Azhar, R., Adzis, N. S., Mohd Ishak, M. A., Ramli, M. Z., Hamzah, M. Y., Ismail, K., & Nawawi, W. I. (2025). Recent updates on TiO_2-based materials for various photocatalytic applications in environmental remediation and energy production. *Desalination and Water Treatment, 321,* 100976.

[48] Tzevelekidis, P., Theodosiou, M., Papadopoulou, A., Sakellis, E., Boukos, N., Bikogiannakis, A. K., Kyriakou, G., Efthimiadou, E. K., & Mitsopoulou, C. A. (2024). Visible-light-activated antibacterial and antipollutant properties of biocompatible Cu-doped and Ag-decorated TiO_2 nanoparticles. *Heliyon, 10*(2), e2434.

[49] Santos-Jr, C. A., Kraka, E., & Moura, R. T. J. (2025). Chemical bond overlap descriptors from multiconfiguration wavefunctions. *Journal of Computational Chemistry, 46*(3), 512–525.

[50] Kanjal, M. I., Afzal, M. W., Sabir, S., Yasmin, I., Li, H.-Y., Luo, H., Song, L.-J., Pang, J.-Y., Bai, Y., & Dang, D.-B. (2025). Dual-step construction of oxygen-vacancy-rich TiO_2 for efficient visible-light desulfurization. *Separation and Purification Technology, 377,* 134268.

[51] Réty, B., Yiin, H.-Y., & Matei Ghimbeu, C. (2025). Quantification of activated carbon functional groups and active surface area by TPD-MS and their impact on supercapacitor performance. *Energy Storage Materials, 74,* 103963.

[52] Gao, Z., Yuan, B., Qi, C., Liu, J., Zhu, Y., Wu, S., Wang, P., Kong, Y., Jin, H., & Mu, B. (2024). Multi-stage releasing water: The unique decomposition property makes attapulgite function as an unexpected clay mineral-based gas source in intumescent flame retardant. *Composites Part A: Applied Science and Manufacturing, 178,* 108014.

[53] Zakusylo, R., Pavlenko, O., Jarosz, T., Maranda, A., Zakusylo, D., & Stolarczyk, A. (2024). Study of the thermal decomposition process of explosive mixtures based on hydrogen peroxide. *Molecules, 29*(23), 5616.

[54] Albin Zaid, Z. A., & Otaru, A. J. (2025). Thermal decomposition of date seed/polypropylene homopolymer: Machine learning CDNN, kinetics, and thermodynamics. *Polymers, 17*(3), 307.

[55] Ahmadlouydarab, M., Javadi, S., & Adel Alijan Darab, F. (2023). Evaluation of thermal stability of TiO_2 applied on the surface of a ceramic tile to eliminate methylene blue using silica-based doping materials. *Advanced Journal of Chemistry, Section A, 6*(4), 352–365.

[56] Maqsood, K., Jamil, A., Ahmed, A., Sutisna, B., Nunes, S., & Ulbricht, M. (2023). Effect of TiO_2 on thermal, mechanical, and gas separation performances of polyetherimide-polyvinyl acetate blend membranes. *Membranes, 13*(2), 121.

[57] Bansal, A., Kumar, A., Kumar, P., Bojja, S., Chatterjee, A., Ray, S., & Jain, S. (2015). Visible light-induced surface initiated atom transfer radical polymerization of methyl methacrylate on titania/reduced graphene oxide nanocomposite. *RSC Advances, 5,* 45645–45654.

[58] El Mchaouri, M., Mallah, S., Abouhajjoub, D., Boumya, W., Elmoubarki, R., Essadki, A., Barka, N., & Elhalil, A. (2025). Engineering TiO_2 photocatalysts for enhanced visible-light activity in wastewater treatment applications. *Tetrahedron Green Chemistry, 6,* 100084.

[59] Arif, M., Javed, M., & Akhter, T. (2024). Crosslinked polymeric networks of TiO_2–polymer composites: A comprehensive review. *RSC Advances, 14*(4), 2001–2022.

[60] Kankala, R. K., Wang, S.-B., Chen, A.-Z., & Zhang, Y. S. (2018). Self-assembled nanogels: From particles to scaffolds and membranes. In J. Conde (Ed.), *Handbook of Nanomaterials for Cancer Theranostics* (pp. 33–62). Elsevier.

[61] Hamiche, A., Yahiaoui, I., Assadi, A. A., Aldrdery, M., Khezami, L., Algethami, J. S., Manseri, A., Elfalleh, W., Amrane, A., & Aissani-Benissad, F. (2025). Degradation of paracetamol by TiO_2-PC500 immobilized cellulosic paper coupling with peroxydisulfate under UV irradiation. *Euro-Mediterranean Journal for Environmental Integration, 10*(4), 2095–2109.

[62] Vaiano, V., Sacco, O., & Matarangolo, M. (2018). Photocatalytic degradation of paracetamol under UV irradiation using TiO_2–graphite composites. *Catalysis Today, 315,* 230–236.

[63] Zul Adlan Mohd Hir, N. N. A., Ahmad Rafaie, H., & Pam, A. A. (2024). Effect of TiO_2 content in activated carbon-supported TiO_2 for paracetamol degradation under low intensity UVC light. *Malaysian Journal of Chemistry, 26*(6), 72–80.

[64] Safitri, V., Santoni, A., Wellia, D., Khoiriah, K., & Safni, S. (2017). Degradation of paracetamol by photolysis using C–N-codoped TiO_2. *Molekul, 12*(2), 189–196.

[65] Pinna, M., Zava, M., Grande, T., Prina, V., Monticelli, D., Roncoroni, G., Rampazzi, L., Hildebrand, H., Altomare, M., Schmuki, P., Spanu, D., & Recchia, S. (2024). Enhanced photocatalytic paracetamol degradation by NiCu-modified TiO_2 nanotubes: Mechanistic insights and performance evaluation. *Nanomaterials, 14*(19), 1577.

[66] Ruziwa, D. T., Oluwalana, A. E., Mupa, M., Meili, L., Selvasembian, R., Nindi, M. M., Sillanpää, M., Gwenzi, W., & Chaukura, N. (2023). Pharmaceuticals in wastewater and their photocatalytic degradation using nano-enabled photocatalysts. *Journal of Water Process Engineering, 54,* 103880.

[67] Greco, E., De Spirt, A., Miani, A., Piscitelli, P., Trombin, R., Barbieri, P., & Marin, E. (2025). Nanomaterials in photocatalysis: An in-depth analysis of their role in enhancing indoor air quality. *Applied Sciences, 15*(3), 1629.

[68] Pavel, M., Anastasescu, C., State, R.-N., Vasile, A., Papa, F., & Balint, I. (2023). Photocatalytic degradation of organic and inorganic pollutants to harmless end products: Assessment of practical application potential for water and air cleaning. *Catalysts, 13*(2), 380.

[69] Terao, S., & Murakami, Y. (2024). Formation of OH radicals on $BiVO_4$– TiO_2 nanocomposite photocatalytic film under visible-light irradiation: Roles of photocatalytic reduction channels. *Reactions, 5*(1), 98–110.

[70] Ghalehkhondabi, V., Fazlali, A., & Soleymani, M. (2022). Folic acid-conjugated pH-responsive poly(methacrylic acid) nanospheres for targeted delivery of anticancer drugs to breast cancer cells. *Journal of Molecular Liquids, 348,* 118028.

[71] Chauke, N. M., Mohlala, R. L., Ngqoloda, S., & Raphulu, M. C. (2024). Harnessing visible light: Enhancing TiO_2 photocatalysis with photosensitizers for sustainable and efficient environmental solutions. *Frontiers in Chemical Engineering, 6,* 1420393.

[72] Singh, J., & Nayak, P. (2023). pH-responsive polymers for drug delivery: Trends and opportunities. *Journal of Polymer Science, 61*(6), 644–660.

[73] Liu, Z., Wang, W., Xie, R., Ju, X.-J., & Chu, L.-Y. (2016). Stimuli-responsive smart gating membranes. *Chemical Society Reviews, 45*(3), 460–475.

[74] Wankhede, S. A., & Barik, A. (2021). Preparation of TiO_2 nanoparticles and its use in wastewater treatment. *International Journal of Engineering Research & Technology (IJERT), 9*(4), 226–230.